Available online at www.sciencedirect.com
SCIENCE DIRECT
Polymer 46 (2005) 12595–12606
polymer
www.elsevier.com/locate/polymer

Crystallization and morphological features of syndiotactic polystyrene induced from glassy state

Chi Wang *, Chang-Chun Lin, Chia-Ping Chu

Department of Chemical Engineering, National Cheng Kung University, 1, University Road, Tainan 70101, Taiwan, ROC

Received 10 June 2005; received in revised form 10 October 2005; accepted 23 October 2005
Available online 14 November 2005

Abstract

Spherulitic growth rates and microstructure of syndiotactic polystyrene (sPS) cold-crystallized isothermally at various temperatures, T_c (115–240 °C), have been investigated by small-angle light scattering (SALS), optical microscopy and transmission electron microscopy. The derived activation energy for sPS chain mobility at the crystal growing front is 5.4 kJ/mol, which is relatively lower than that of isotactic polystyrene, 6.5 kJ/mol. In addition, the Hv scattering invariant (Q_{Hv}) measured by SALS on the crystallized sPS samples displays a pronounced minimum at ~150 °C. Despite a wide range of T_c used, however, the sample crystallinity estimated by Fourier transformation infrared spectroscopy remains unchanged. Prior to crystallization, the correlation length derived from the Vv patterns on the basis of Debye–Bueche model is ca. 1.13 μm regardless of T_c used. Interconnected domains with a width of ca. 1.8 ± 0.5 μm are readily observed in all the crystallized samples under phase contrast microscopy and the phase-separated structure is conserved within sPS spherulites whose diameters are increased with increasing T_c.

Based on the above facts, we conclude that the presence of a Q_{Hv} minimum is ascribed to the resultant events of the two competitive transitions i.e. liquid–solid crystallization, and liquid–liquid demixing resulting from the spinodal decomposition (SD). At lower T_c, the unstable SD transition overwhelms the crystallization. Despite the low chain mobility, the coarsening process driven by the interfacial energies has reached a certain level before crystalline nucleation takes place. At higher T_c, on the other hand, cold crystallization becomes the dominant process due to the enhanced chain mobility, leading to the suppression of ongoing SD coarsening process. At an intermediate T_c range, comparable competition of the phase separation and crystallization prohibits the development of ordered symmetry within spherulites, giving the presence of Q_{Hv} minimum.

Keywords: Phase separation; Cold crystallization; Syndiotactic polystyrene

1. Introduction

When crystallized from the melt, sPS chains will pack themselves into two possible crystalline forms due to the polymorphic nature, i.e. hexagonal α and/or orthorhombic β forms, depending on the cooling rate and pre-melting temperatures [1,2]. For β-form sPS samples, both spherulites and axilites are discernible and the relative population is dependent upon crystallization temperature [3]. Majority of the β-form spherulites possess positive birefringence but occasional spherulites with negative birefringence have been identified, indicating the difference in the lamellar orientation [3]. In contrast, tiny spherulites with no birefringence are recognized in α-form sPS samples [4]. The crystallization kinetics has been extensively studied via differential scanning calorimetry (DSC) [5–8] and polarized optical microscopy (POM) [3,9,10]. Previously, we reported the first small-angle light scattering (SALS) results on the subject of melt-crystallization kinetics based on the invariant approach [11]. On the other hand, less attention was paid to the kinetics of sPS crystallized from the glassy state [5,6]. At present, crystal growth rates of sPS at temperatures near its glass transition temperature (95 °C) have not been reported yet. Although POM is widely used to measure the growth rates of spherulites, difficulties are frequently encountered when the morphological entity is too small to be resolved by the optical microscopy. Small diameter spherulites (ca. ~5 μm) with dense population are generally found for polymers crystallized from the glassy state, leading to the infeasible application of POM for measuring the spherulitic growth. Instead, benefits can be obtained using SALS to trace the growing spherulites. To complement and compare with our previous studies [11], an

* Corresponding author. Tel.: +886 6 2757575x62645; fax: +886 6 2344496.
E-mail address: chiwang@mail.ncku.edu.tw (C. Wang).

0032-3861/$ - see front matter © 2005 Elsevier Ltd. All rights reserved.
doi:10.1016/j.polymer.2005.10.122

attempt has been made in this work to carry out SALS measurements to proceed the series kinetics study of sPS crystallization from the glassy state.

During the course of sPS cold crystallization, we also observed a peculiar spherulitic morphology, exhibiting interconnected domains embedded within the well-defined spherulites which is reminiscent of spinodal decomposition (SD) phase separation preserved after crystallization. Conventionally, it is suggested that phase separation will take place in a multi-component blend in which the constituents become immiscible under a specific condition. However, evidences have been provided recently to support (or debate) a new hypothesis that phase separation induced by SD in one-component semicrystalline polymers might take place prior to the formation of stable nuclei under appropriate conditions set in the system [12–18]. In one-single component, it is thought that conformation ordering coupled with density fluctuations is the main event to account for the spinodal decomposition involving two phases; one has the preferential conformation for subsequent crystallization, the other remains amorphous due to the random conformation distribution. Using Hv configuration of light scattering to investigate the structure development prior to crystallization, Kaji et al. [19] inferred from the observed logarithmic intensity increases with elapsed time that SD takes place before sPS nucleation. Complemented with Fourier transformation infrared spectroscopy (FTIR) results which show that the amount of trans conformation increases during the induction period, they suggest that spinodal-assisted crystallization is an appropriate model to account for what they obtained.

In this work, we pay special attention to the temperature effect on the sPS morphology developed near T_g and emphasis is given to discuss the two plausible transitions; i.e. liquid–solid (cold crystallization) and liquid–liquid (phase separation) transitions. Based on our findings, it is of importance to realize two facts; the first is the existence of Hv-invariant minimum (Fig. 10) at an intermediate temperature, and the second is the appearance of the SD-like phase structure under phase contrast microscopy. Our results seem to further support the previous work [19], suggesting that SD phase separation indeed takes place in the single-component sPS when heated from the glassy state. Possible explanations will be explored. In addition, the Williams–Landel–Ferry (WLF) parameters for describing the activation energy and ceasing temperature for sPS chain motion are derived from the growth rate results on the basis of the classical crystallization theory.

Our results for the sPS studied are new since no detailed microstructure and spherulitic-growth-rate data of cold-crystallized sPS have been reported.

2. Experimental

sPS pellets with a weight-average molecular weight ~200 k were used in this study. Samples with a thickness of ~20 μm were prepared by hot press. The as-pressed samples were then heated to 300 °C for 10 min and then quenched in liquid nitrogen to obtain amorphous sPS for subsequent cold-crystallization studies. The quenched samples were transparent with no voids. Wide-angle X-ray diffraction (WAXD) patterns showed no trace of crystallinity in these samples. Amorphous state of these samples was also confirmed by the absence of any absorbance band at 1222 cm^{-1} under FTIR. The band at 1222 cm^{-1} is assigned to the all-trans conformation in the crystals and its intensity is associated with the degree of crystallinity developed [20]. FTIR was performed using a FTIR Microscope (Perkin–Elmer, Spectrum one).

Amorphous specimens were placed in a Linkam THMS600 hot stage and heated at a rate of 100 °C/min to the desired crystallization temperature, T_c, for isothermal crystallization. The specimen was illuminated by a polarized He/Ne laser light

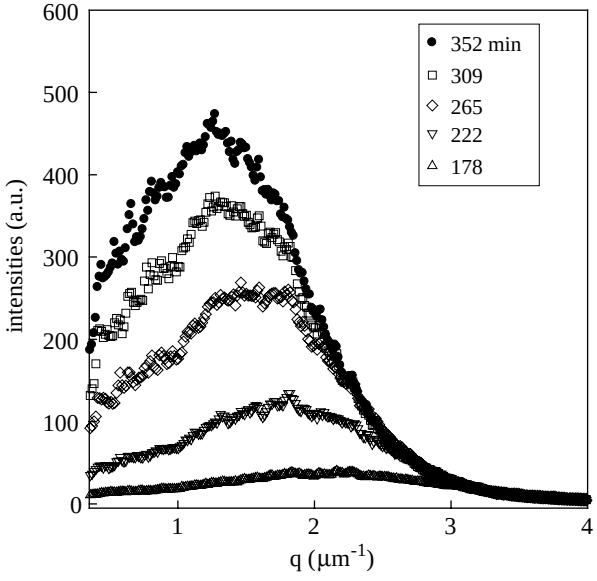

Fig. 1. Change in Hv light-scattering profiles at azimuthal angle 45° of amorphous sPS samples with time after the temperature jump from room temperature to 117.5 °C.

(4 mW) and the scattering pattern was visualized on a screen, which was further recorded using a highly sensible CCD camera (Apogee, AP1). Time-resolved SALS were conducted under Hv polarization mode to trace the evolution of anisotropy fluctuation as well as Vv polarization mode to reveal the variation of correlation length during measurements. To observe the detailed morphology directly, a POM (Leica, DMLP) equipped with phase contrast lens was used. To characterize the crystal form of the crystallized sPS, WAXD experiments were conducted using a Rigaku Dmax2000 with a Cu target. The crystal modification was also characterized using FTIR which provided more appropriate information than WAXD, by which the short-range crystal order developed normally in the cold-crystallized sPS might not be detected appropriately [21]. Variations in sample thickness were normalized by measuring the integrated intensity of the conformationally insensitive band at 1601 cm^{-1}, which is attributed to the benzene ring stretching vibrations [20,21]. Thus, the relative crystallinity developed at selected T_c can be quantified in terms of the reduced factor obtained from the peak area ratio of 1222 to 1601 cm^{-1} band after appropriate peak separations. Thin sections, ca. 50 nm thick, of the crystallized samples were prepared for transmission electron microscopy (TEM) observations using an Ultracut UCT (Leica) microtome. Staining of the thin sections was carried out at room temperature with ruthenium tetraoxide vapors. TEM experiments were performed using a JEM-1200EX (Jeol) microscope operated at 80 kV.

3. Results and discussion

3.1. Crystallization kinetics studies

Four-leaf-clover scattering patterns of Hv configuration were obtained during sPS cold crystallization in the temperature range 115–240 °C studied, implying the development of spherulites within samples. Typical one-dimensional Hv scattering profiles at an azimuthal angle 45° is shown in Fig. 1, where the scattering maximum is evident. The scattering angle ($2\theta_{max}$) associated with the intensity maximum of the four-leaf-clover scattering pattern was determined and used to calculate the spherulitic radius (R) by means of the relation [22]: $R = 4.08/q_{max}$, where q is the scattering vector and defined as $q = 4\pi/\lambda \sin(\theta)$. Fig. 2 shows the variation of spherulitic radius with time (t_c) for samples cold-crystallized at various T_c. Spherulitic growth rates (G) were determined from the linear slopes. As shown in Fig. 3, the growth rate is accelerated at high T_c due to the enhanced chain mobility. When T_c is above 150 °C, crystallization rate is such high that trace of the evolution of Hv scattering patterns becomes infeasible. It is consistent with the DSC heating trace of the glassy sPS where a crystallization exothermic peak is located at ca. 149.2 °C. In addition to the growth rate results, crystallization kinetics are also conveniently discussed in terms of the Hv scattering invariant Q_{Hv}, defined as $Q_{Hv}(t_c) = \int_0^\infty I_{Hv}(q, t_c) q^2 dq$ [23], together with the Avrami equation. Fig. 4 shows the time evolution of measured Q_{Hv}, which are normalized with that obtained after complete crystallization Q_{max}. The Avrami equation has been frequently used to analyze the crystallization kinetics of polymers [24],

$$Q_{Hv}(t_c)/Q_{max} = 1 - \exp[-k(t_c - t_0)^n] \quad (1)$$

where k is the overall crystallization rate constant, n is the Avrami component and t_0 is the induction time of crystallization process. The induction time is significantly reduced at high T_c. The crystallization half-time, $t_{1/2}$, is defined as the time required for the system to reach one half of the relative conversion ($Q_{Hv}/Q_{max} = 0.5$). A simple relation between these Avrami parameters is expressed by $(\ln 2/k)^n = 1/t_{1/2}$. Due to its convenient derivation, $1/t_{1/2}$ is an appropriate parameter to describe the relative rate of crystallization process [8]. The values of $t_{1/2}$ at various T_c are also included in Fig. 3, along with G values for a detailed comparison of crystallization kinetics. Similar with the trend of the induction time, $t_{1/2}$ also decreases with increasing T_c, suggesting a fast crystallization process at high T_c.

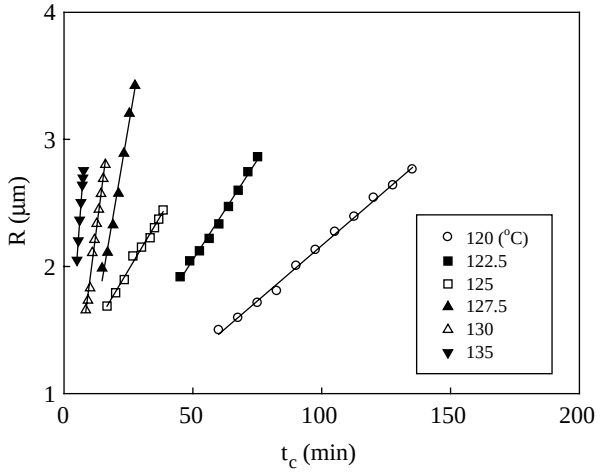

Fig. 2. Time variation of spherulitic radius determined from Hv light-scattering profiles.

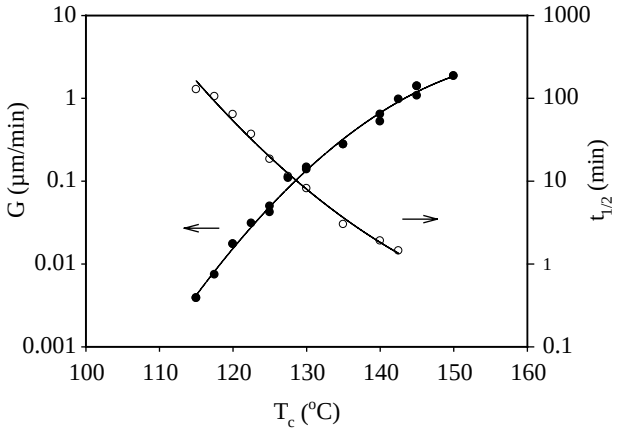

Fig. 3. Temperature dependence of linear crystal growth rate, G, and crystallization half-time, $t_{1/2}$, obtained from SALS.

When crystallization takes place at high supercooling, nucleation of stable crystals occurs readily but the mobility of sPS chains is virtually low, leading to a diffusion control process. At T_c not far from T_g ($T_g < T_c < T_g + 100$ °C), the activation energy of the sPS chain diffusion is generally described by the WLF type [25]. Thus, the T_c dependence of G can be expressed by Eq. (2).

$$G(T_c) = G_0 \exp\left[\frac{-\Delta E_{WLF}}{R(T_c - T_\infty)}\right] \quad (2)$$

where G_0 is a constant, ΔE_{WLF} is the WLF-type activation energy for transport of segments to the crystallization site, and T_∞ is the temperature below which the segmental motion ceases and is expressed as $T_g - C$, where C is a constant depending on the polymer types. According to Eq. (2), three parameters (G_0, ΔE_{WLF} and C) are needed for describing the T_c-dependence of the growth rates. To induce reliable parameters, we first choose an appropriate C value and then carry out the linear regression of the plot of ln G versus $1/(T_c - T_\infty)$ to determine the corresponding G_0 and ΔE_{WLF} values. At the given C value, thereafter, summation of the difference between the experimentally-measured G and theoretical value calculated by Eq. (2), i.e. $\sum (G_{exp} - G_{cal})^2$, is calculated. The variation of derived summations with selected C values is shown in Fig. 5, where a shallow broad minimum is found around 26 ± 4 °C, representing the best fit. The derived optimal C value is close to the reported value for isotactic PS (~30 °C) based on a similar procedure [26]. Miyamoto et al. [27] obtained a slightly higher C value (~39 °C) for iPS on the growth rate studies at a wide temperature range. Based on either G or $1/t_{1/2}$ results, good agreement with Eq. (2) is reached as shown in Fig. 6 and from the slope the derived ΔE_{WLF} is ca. 5.4 kJ/mol, which is slightly smaller than that of iPS (6.5 kJ/mol) obtained by Suzuki and Kovacs [26]. Without specification of the C value, Okamoto et al. [28] derived an activation energy of 6.1 kJ/mol for sPS using crystallization-half times derived from their SALS results. For atactic PS, on the other hand, the WLF parameters obtained from the bulk viscoelastic properties are significantly distinct from those of sPS and iPS [29,30]. Since, chain motion takes place locally at the crystal growing front, as pointed out by Mandelkern [31], ΔE_{WLF} and C values derived from crystallization kinetics are not necessarily the same as those obtained from the bulk properties. It is also worthwhile to note in Fig. 6 that the DSC data taken from Wu and Woo [6] superimpose with our SALS data, suggesting the consistence of kinetics analyses. The derived ΔE_{WLF} is similar using the data obtained from G, $t_{1/2}$ or $k^{1/n}$ measurements. The Avrami exponent derived from DSC

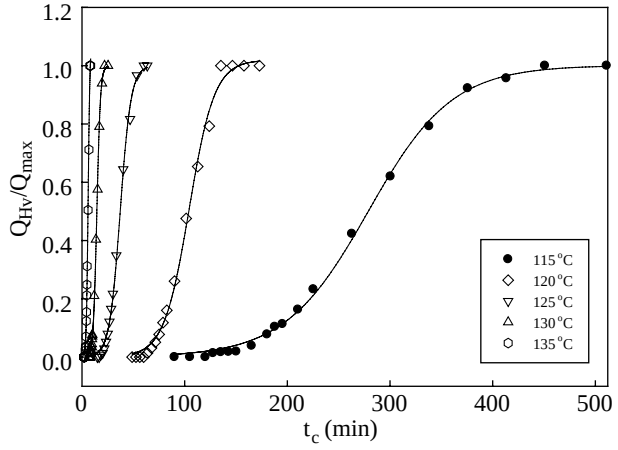

Fig. 4. Time variation of light-scattering invariant Q_{Hv} for sPS cold-crystallized at various T_c.

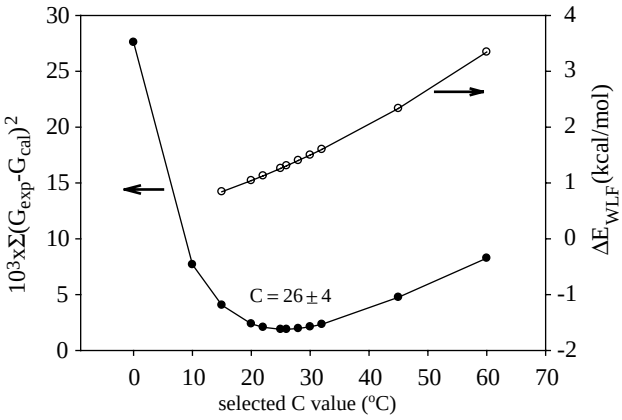

Fig. 5. Optimal determination of the C value to minimize the discrepancy between the experimentally-measured and theoretically-estimated G values.

[6] or SALS (Fig. 4) results is ca. 3.0, suggesting three-dimensional growth of sPS spherulites with heterogeneous nucleation. A similar deduction for the melt-crystallized sPS samples has also been obtained previously [11]. Through a simple relation, $k=(4\pi/3)NG^3$, the nucleation density N is calculated to be 0.24 μm^{-3}, which is ca. 2–3 order higher than those for sPS samples crystallized from the melt state [11]. In contrast with cold-crystallization, larger spherulites with diameters ranging from 15 to 30 μm have been obtained for sPS samples met-crystallized in the T_c range of 247–267 °C due to the lower nucleation density [3].

3.2. Structure developed from cold crystallization

After complete crystallization at various T_c, the crystallized samples were investigated using SALS, OM, FTIR, WAXD and TEM at room temperature to reveal the structural development. Fig. 7 shows the typical SALS patterns and phase-contrast optical micrographs of sPS samples cold-crystallized at three typical T_c. Based on the Hv scattering patterns, spherulitic entities within samples are evident and the spherulitic diameter is larger at higher T_c. The Vv scattering patterns exhibit characteristics of positively birefringent spherulites. Under POM observation, spherulitic features are readily found; most of them are positively birefringent but sporadic appearance of spherulites with negative birefringence is also found. The origin to render the difference in the birefringence characteristics is ascribed to the lamellar orientation within the spherulites, as pointed out previously [3]. It is of interest to note that the spherulitic anisotropy seems to diminish for samples crystallized at $T_c=145$ °C on the basis of Vv scattering pattern where only a circular symmetric intensity profile is discernible. Fig. 8 shows the $I_{Hv}q^2$–q plots for samples crystallized at the selected T_c, of which the Hv scattering patterns are shown in Fig. 7(a). Indeed, the anisotropy of spherulites characterized by the Hv invariant (determined from the area underneath the curves) is significantly lower at 145 °C than those at the other two temperatures, indicating the T_c-dependence of structural variation within spherulites.

Under phase contrast microscopy (Fig. 7(c)), moreover, it is also of importance to observe the existence of interconnected domains regardless of T_c used. The modulated morphology is reminiscent of SD phase separation structure developed in the two-component polymer blends. The interconnected domains, however, do not give rise to the typical ring pattern in the Vv

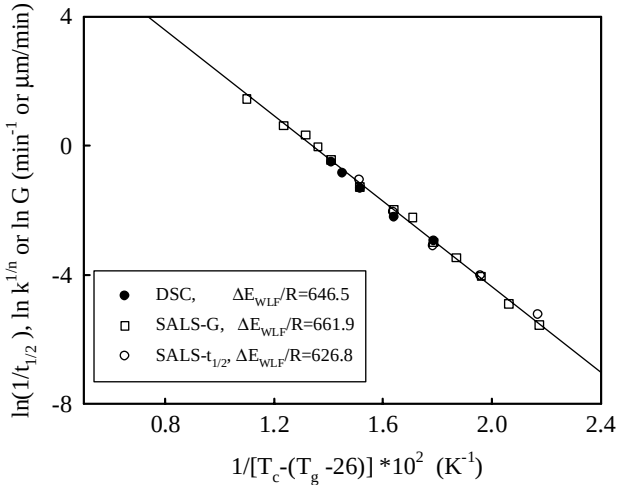

Fig. 6. Comparison of crystallization kinetics analyzed using various approaches (●, DSC kinetics with measured k and n; ○, SALS with measured G values; △, SALS with Q_{Hv} and $t_{1/2}$ values).

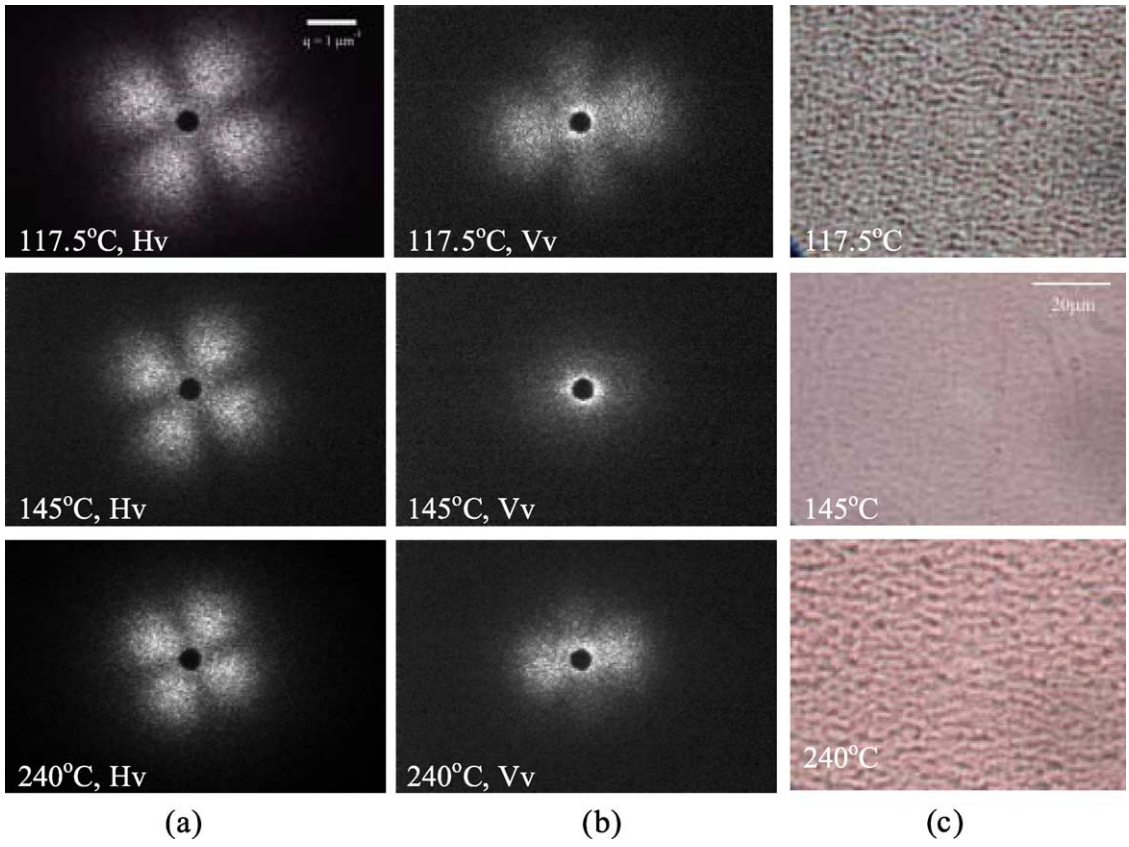

Fig. 7. (a) Hv, (b) Vv scattering patterns and (c) phase contrast micrographs of sPS cold-crystallized at various T_c.

scattering mode as always being found in the phase-separated blend systems, indicating the weak scattering intensity, which might be obscured by the relatively strong background scattering. The modulated morphology becomes rather vague at $T_c = 145$ °C, compared with those at the other two temperatures. Two-dimensional fast Fourier transforms (FFT) of the OM micrographs were conducted and the periodic wavelengths (Λ) of the modulated structure were obtained from the spinodal rings. The T_c-dependence of Λ is displayed in Fig. 9. Also given in Fig. 9 are the domain widths measured from the optical micrographs (Fig. 7(c)) and the spherulitic diameters determined from the Hv scattering patterns (Fig. 7(a)). Both Λ and spherulites increase slightly with increasing T_c and the Λ value is always about two times smaller than the diameter of spherulite. Indeed, careful inspection on the POM micrographs leads to the conclusion that each individual spherulite is composed of phase-separated domains inside. Similar SD morphology and Λ have been reported for neat poly(ethylene terephthalate) crystallized from the glassy state [32].

To quantitatively characterize the spherulites developed at each T_c, the Hv invariants of completely crystallized samples (Q_m) were determined and the T_c-dependence of Q_m was given in Fig. 10, where a pronounced minimum is

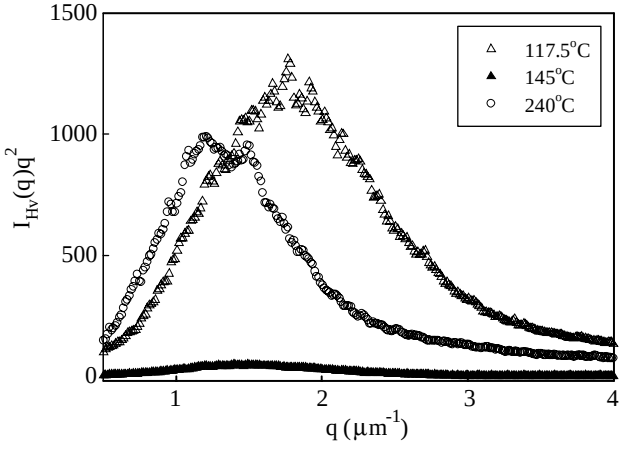

Fig. 8. $I_{Hv}q^2$ versus q plots for samples crystallized completely at various crystallization temperatures.

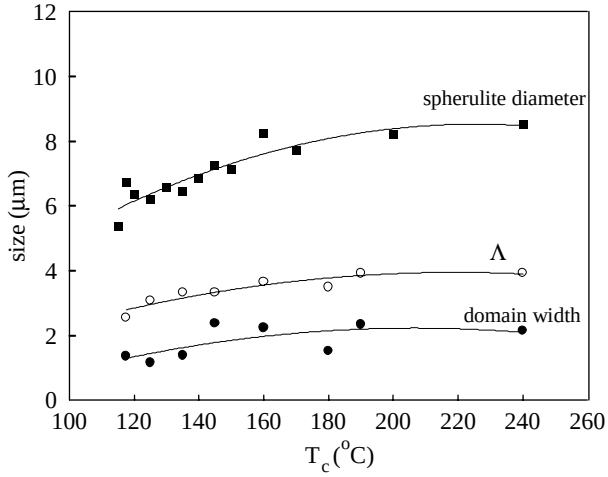

Fig. 9. Spherulite diameter, domain width and characteristic wavelength, Λ, of the phase-separated structure developed at various T_c.

observed at 150 °C and the magnitude of Q_m is ca. 100 times less than those at 115 and 240 °C. For spherulites embedded in an isotropic amorphous matrix, invariant Q_{Hv} can be expressed as [23,33]: $Q_{Hv} \approx \phi_{sp}(\delta_{cr}^0 \phi_{c,sp} P_2)^2$, where ϕ_{sp} is the volume fraction of spherulites, $\phi_{c,sp}$ is the volume fraction crystallinity within the spherulite, δ_{cr}^0 is the intrinsic anisotropy of pure crystals and P_2 is a Hermans-type orientation function describing the crystal orientation with respect to the radius of the spherulite. When isothermal crystallization is complete, spherulites become volume filling, i.e. $\phi_{sp}=1.0$, according to our POM observations. Provided that there is no variation of crystal modifications, Q_{Hv} becomes dependent merely upon $\phi_{c,sp}$ as well as P_2. To distinguish the individual effect of $\phi_{c,sp}$ from P_2 on the measured Q_m, sample crystallinities were estimated by the $A_{1222\ cm^{-1}}/A_{1601\ cm^{-1}}$ ratio obtained from FTIR results (Fig. 11(a)) and were displayed in Fig. 10 as well. It is of interest to note that the crystallinity remains unchanged for samples crystallized at T_c from 115 to 220 °C, which is consistent with WAXD results (Fig. 11(b)) and previous findings by Musto et al. [21]. Moreover, the sPS crystal modification judging from FTIR and WAXD is concluded as follows: mesomorphic phase of sPS is found at T_c lower than 130 °C; only α-form sPS is developed at 130 °C $< T_c <$ 180 °C; for $T_c >$ 180 °C, majority of the crystals are in the α-form but small trace of β-form sPS is occasionally detected [34]. Previous studies [35,36] showed that the mesophase and α-form sPS are the main species developed in the cold-crystallized samples regardless of the crystallization temperature, and the former can serve as a template for growth of the later. It has been shown that the mesomorphic form of sPS indeed is constituted of small and imperfect crystals of the α crystalline form [37]. Its crystalline structure possesses only short-range order with no long-range order, verifying by the presence of absorbance band at 1224 cm^{-1} (Fig. 11(a)) but the absence of any sharp diffraction peaks in the WAXD patterns except a huge hump at $2\theta \sim 20°$ (Fig. 11(b)). On the basis of FTIR and WAXD results, both $\phi_{c,sp}$ and δ_{cr}^0 are assumed intact at least for samples crystallized at T_c from 110 to 180 °C. Thus, the presence of Q_m minimum as shown in Fig. 10 is simply relevant with the reduction of lamellar orientation

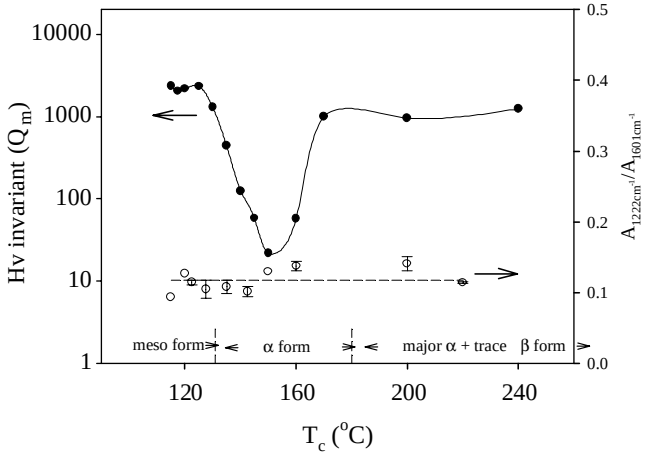

Fig. 10. Variation of Hv invariants and relative crystallinities of sPS cold-crystallized at various T_c. The reduced absorbance, 1222 cm^{-1}/1601 cm^{-1} measured by FTIR represents the relative crystallinity of the sample. The crystal forms are determined from the FTIR and WAXD results.

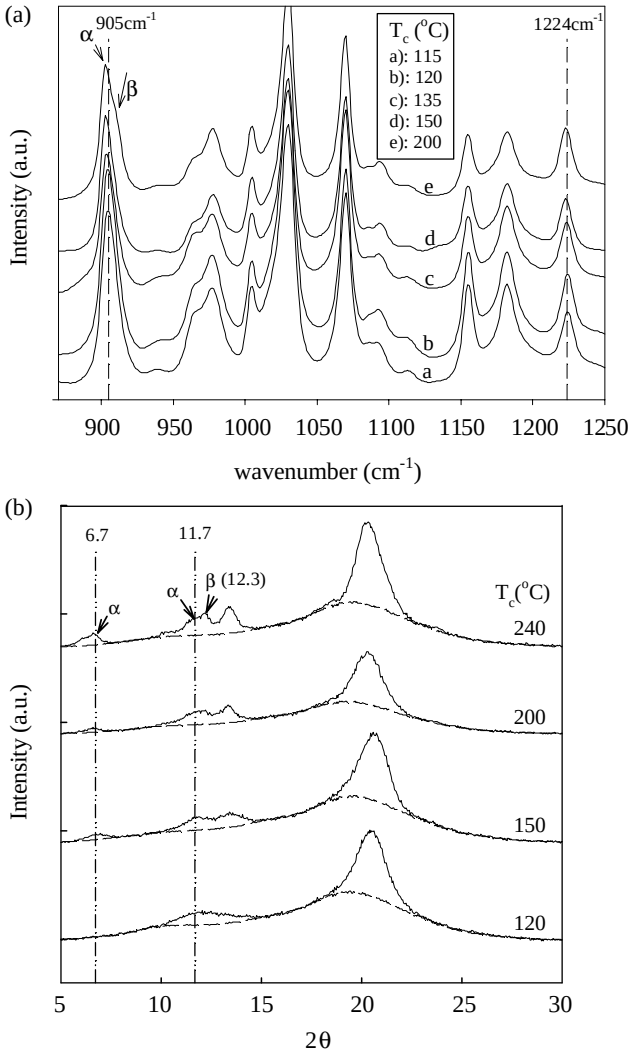

Fig. 11. (a) FTIR spectra and (b) X-ray diffraction profiles of sPS samples cold-crystallized at various crystallization temperatures, T_c. The dashed lines in (b) are the contribution of the amorphous phase and the crystallinity index is then determined from the ratio of the integrated intensity in the crystalline peaks to the total area of coherent scattering. The absorbance peaks at 902 and 911 cm^{-1} are due to the α- and β-form crystals, respectively, and the absorbance peak at 1224 cm^{-1} is associated with the chains in planar zig-zag conformation. Diffraction angles (2θ) at 6.7 and 11.7° are indicative of the presence of α-form crystals, whereas β-form crystals give rise to the appearance of diffraction peaks at $2\theta = 12.3°$. Mesomorphic samples are different from the amorphous ones mainly due to the presence of the FTIR band at 1224 cm^{-1}.

within spherulites, reflecting by one order less in the P_2 magnitude.

3.3. Lamellar morphology of cold-crystallized samples

As shown in Fig. 12 are the lamellar morphologies observed under TEM for sPS samples crystallized at different T_c. The dark regions which have been effectively stained by RuO_4 represent the amorphous phase, whereas the bright regions correspond to lamellar crystals. Lamellae with short lateral dimensions are found in all the cold-crystallized samples in contrast with those developed in the melt-crystallized sPS where long and parallel lamellae are detected [38]. Despite the development of imperfect α-form crystals, thin lamellae (thickness $\sim 4.0 \pm 0.9$ nm) with good orientation are still observed within samples crystallized at 120 °C. At higher T_c, the lamellae are thicker and become more discernible resulting from the perfection of crystals. The thicknesses of lamellae developed at 150, 200 and 240 °C are 5.6 ± 1.0, 5.7 ± 1.3, and 5.7 ± 1.2 nm, respectively.

3.4. What happens during the induction period of crystallization ?

It has been known that the radius of gyration of polymer chains remains unchanged before and after crystallization, suggesting the relevance of segmental mobility in determining the liquid–solid phase transition. Without large-scale molecular motion of the backbone chains to induce crystallization, chain segments with correct conformations are believed to be able to trigger an ordering process, leading to an increase of the persistent length gradually. Coupling with inter-chain ordering simultaneously, crystal nuclei are produced and crystal growth is followed subsequently. In other words, domains having

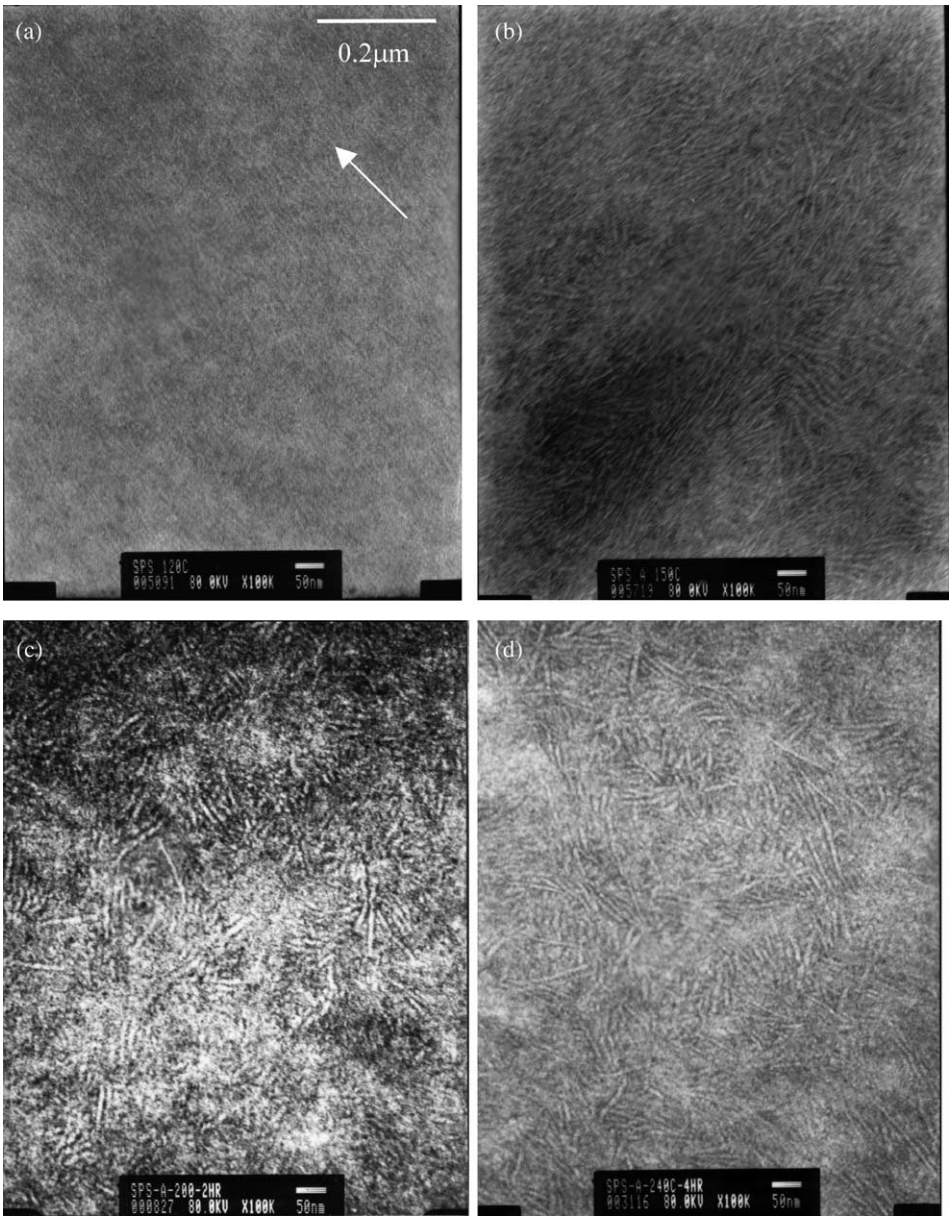

Fig. 12. TEM images of sPS cold-crystallized at (a) 120 °C, (b) 150 °C, (c) 200 °C, (d) 240 °C. The arrow in (a) pointing the growth direction of lamellae.

specific conformations are the precursors of subsequent crystal nucleation. Based on this conformation-density coupling concept, Olmsted et al. [15] have discussed the plausible existence of liquid–liquid phase transition in the neat polymer prior to crystallization. Since, no activation energy is required for the SD process, it is expected that early stage of SD eventually takes place prior to the cold crystallization where a critical energy is necessary to forming stable sPS crystal nuclei.

Kaji's group [17,19] has been studied the phase transition of sPS from glassy state before the initiation of crystallization. Based on the logarithmic increase of Hv intensities with elapsed time, they proposed that SD phase transition takes place in neat sPS immediately at the elevated temperature. They have suggested that orientational ordering process coupled with density fluctuation takes place during the induction period, which may serve as a precursor to the subsequent crystallization. Based on the FTIR and depolarized light scattering results, they concluded that three stages can be distinguished [17], particularly through the process of spinodal decomposition, prior to sPS crystallization. However, they focused mainly on the structural developments during the induction period and no detailed morphological features and crystal growth rates were provided.

To characterize the structure variation preceding the crystallization, we have carried out a different approach to analyze the SALS data in the induction period. In general, I_{Hv} arises from orientation fluctuations while I_{Vv} results from both orientation and density fluctuations [22,39]. For systems prior to crystallization, the contribution of density fluctuations is dominant in Vv scattering, producing an essentially circular symmetric scattering patterns. Based on Debye–Bueche model, I_{Vv} scattering gives a simple relation with correlation length (ξ)

describing the spatial size of fluctuations [39,40], as follows,

$$I_{Vv}(q) = \frac{A}{(1+\xi^2 q^2)^2} \quad (3)$$

where A is a constant. The ξ value was determined from the square root of the slope/intercept ratio by plotting $I_{Vv}^{-1/2}(q)$ versus q^2. The magnitude of ξ is a characteristic length scale associated with the mean dimensions and volume fractions of the randomly distributed phases. Fig. 13 shows the typical Debye–Bueche plots at different times for sPS crystallized at 115 °C. The application of Debye–Bueche model is confirmed by the linear dependence obtained at the low q regions. Although the I_{Vv} intensity increases with the elapsed time, it is of importance to note that the derived ξ values are identical (ca. 1.13 μm) for t_c up to 150 min. The induction time for crystallization is 150 min, as detected by the Q_{Hv} increment shown in Fig. 4. The increase of I_{vv} intensity during the induction period is consistent with previous results [39], resulting from the occurrence of phase separation. However, the fact of unchanged ξ implies that large-scale coarsening of the phase-separated structure is significantly limited, plausibly due to the high viscosity.

Fig. 14(a) and (b) shows the time evolution of structural development for samples crystallized at 117.5 °C as observed on the same field under an optical microscopy using parallel-polarized and cross-polarized light, respectively. The scale bar is 10 μm, and is the same for all micrographs. The I_{Hv}–q plots at selected t_c are given in Fig. 1 and the time evolution of Hv invariants is displayed in Fig. 14(c) as well. Determined from the initial rise of measured Q_{Hv} in, the crystallization induction time is ca. 110 min, at which the appearance of four-fold symmetry is barely noted (Fig. 1). Moreover, the time required to reach half of crystallinity is 230 min. The arrows in Fig. 14(c) point to the corresponding invariants at the crystallization times given in Fig. 14(a). At the end of cold crystallization, a typical tiny spherulite (diameter ~6 μm) with well-developed Maltese cross is located in the dashed circle (Fig. 14(b)) but the circles marked on Fig. 14(a) merely provide the eye-guide at the same region. For t_c smaller than 50 min, featureless structure is obtained under OM observations but the Vv scattering gives a correlation length of 1.2 μm, suggesting the undergoing phase separation. Until 60–100 min, the bi-continuous phase structure is seen and tiny superstructures with still low anisotropy have developed within the whole samples, indicating the incubation of crystallization. The phase contrast of the bi-continuous phase structure is pronouncedly enhanced (t_c = 120 min) if small amount of crystals (Q_{Hv}/Q_{max} = 0.05) form in the relatively ordered phase. Well-developed tiny spherulites appear at 160 min and spherulitic growth is observed under cross polars, accompanying with the gradual increase of the transmitted light intensities. The phase-separated structure is conserved during the crystallization process (160–300 min) and becomes more distinct towards to the completion of crystallization (420 min).

On the basis of Figs. 13 and 14 together with the results obtained by Kaji et al. [19], we conclude that SD phase separation precedes the crystal formation for sPS samples crystallized from the glassy state. The spatial size of density fluctuation remains unchanged but the contrast of phase-separated structure is enhanced, after small crystals exist in the ordered phase, to give a better observation. The phase-separated structure is conserved within sPS spherulites, indicating by Figs. 9 and 14(a).

3.5. Competition between phase separation and crystallization

At the high-temperature melt state, no preferential conformation of sPS chains is expected rationally, i.e. randomly distribution of trans and gauche conformations in the melt. The randomized structure is preserved if the sample is rapidly quenched to the glassy state. Since, there is no activation energy required for the spinodal decomposition, the melt-quenched samples on heating above T_g will first be demixed to various stages, followed by a subsequent

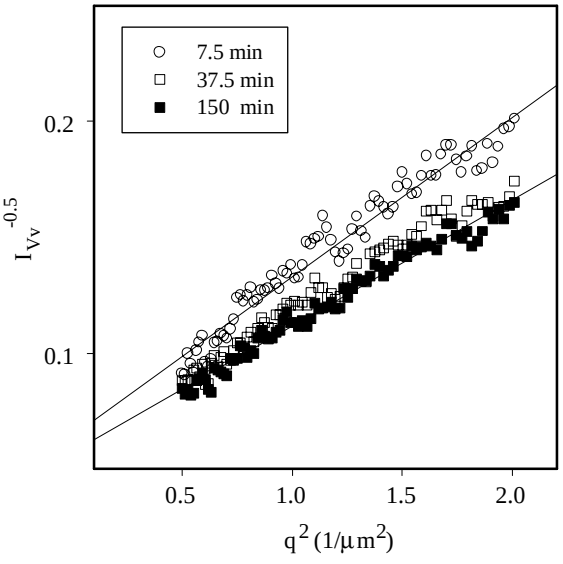

Fig. 13. Debye–Bueche plots of Vv scattering results for sPS cold-crystallized at 115 °C. The crystallization induction time is ca. 150 min determined from Fig. 4.

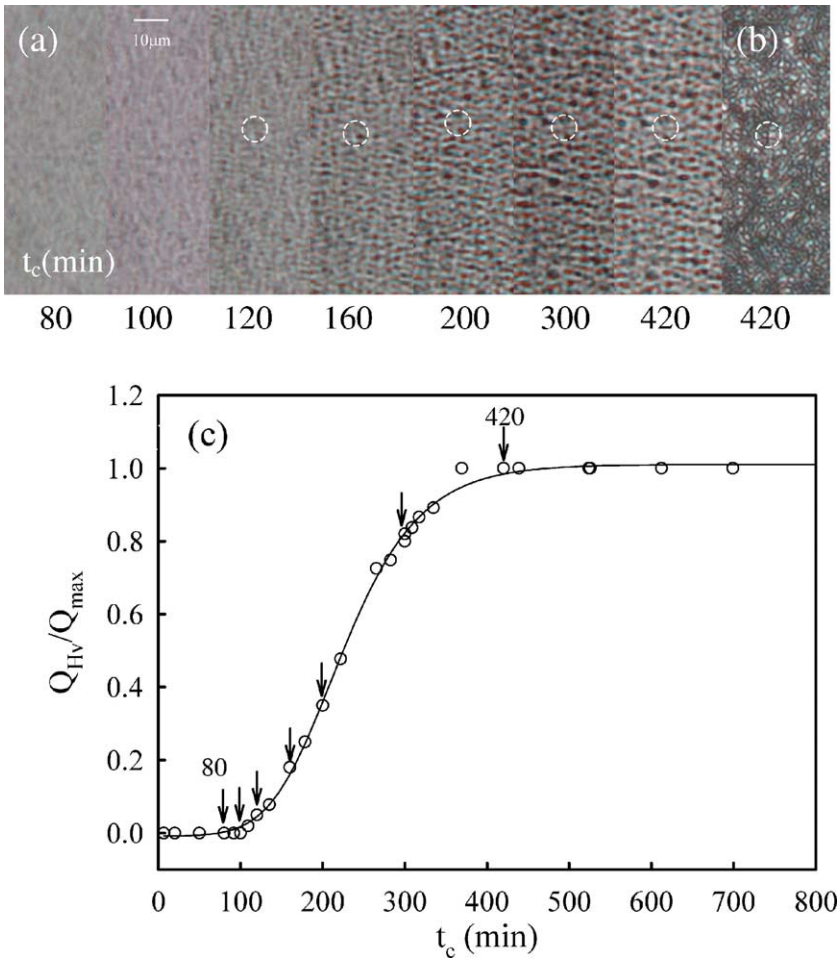

Fig. 14. Morphological evolution of sPS during cold-crystallization at 117.5 °C as-revealed by OM (a) parallel-polarized, (b) cross-polarized configuration and (c) time evolution of Q_{Hv} by SALS. The crystallization induction time is ca. 110 min determined from SALS.

coarsening process. However, crystallization process will be triggered as well under the conditions that mobility of sPS chains is sufficiently high to overcome the energy barrier for diffusion. Thus, the resulted morphology of the cold-crystallized sPS is the outcome of the interplay of two kinds of phase transitions, i.e. liquid–liquid phase separation and liquid–solid crystallization.

When subsequently heated to a temperature slightly higher than T_g (T_c = 115–125 °C), limited mobility is just sufficiently high for sPS chain segments with correct conformation to register one another locally, but not high enough for individual chain motion to develop a stable nuclei via inter-chain co-operativity. Thus, the early stage of SD process starts at the very initial period immediately after the desired T_c is reached. As conformational ordering proceeds, the persistence length is increased and gradually gives rise to the local orientational ordering as mentioned previously by Kaji et al. [19] in their depolarized light scattering results. Interconnectivity of thin domains with correct conformation segments is developed quickly, resulting in the existence of two separated liquid phases with different densities (conformational orders). One of the coexisting phases possesses a lower density than the original liquid, but the other with correct conformation is higher. The denser phase possesses the same conformation (trans sequence) with the crystal phase, leading to the lower activation required to initiate the crystallization than the original liquid. At this stage, Hv and Vv scatterings are appropriate to trace the structural development. But, the phase contrast is too low to observe morphological features under OM until crystallization is about to be initiated. An apparent late stage of SD is observed due to the growth of oriented domains through co-operative motion of neighboring domains. In spite of that insignificant coarsening of the interconnected domains is seen due to the high viscosity, the ordering process in the denser and ordered phase through the conformational arrangement is prevailing, and eventually triggers the formation of stable sPS crystal nuclei. Subsequent growth of lamellar crystals spreads across the phase boundary and the signature of SD is conserved within the spherulites developed since large-scale interchain motion at the crystal front is limited at low T_c. In other word, SD phase transition dominates the morphological development.

At high T_c (165–240 °C), however, the late stage of SD is hardly discernible [17] since a fast crystallization with an extremely short induction time takes place, leading to the

infeasibility of SALS for growth rate measurements. The crystallization rate is so fast that the early stage of SD may be arrested and preserved in the final morphology [41]. The crystallization becomes the dominant transition due to the enhanced chain mobility, leading to the suppression of ongoing SD coarsening process.

At the intermediate T_c (125–165 °C), the rates for the phase separation (coarsening stage) and crystallization are comparable, and these two competing processes result in the randomization of lamellar orientation within spherulites, giving rise to the Q_{Hv} minimum as shown in Fig. 10.

4. Conclusions

SALS was carried out to investigate the structural development of sPS cold-crystallized isothermally at various temperatures, T_c (115–240 °C). The underlying principle of this work is that WLF parameters describing sPS chain mobility at the growing crystal fronts can be derived from the spherulitic growth rates obtained by SALS at temperatures close to the glass transition temperature. For sPS cold-crystallized at various T_c, characteristic features of the morphology observed by phase contrast microscopy are regular and interconnected phases with a periodic distance of about 3.4 μm. The morphology is rather similar in appearance to that usually found in the SD phase separation structure. The phase-separated domain width was independent of the temperature T_c, being 1.8 ± 0.5 μm, whereas the spherulite diameter increased from 5.3 to 8.5 μm as T_c increased from 115 to 240 °C. It was found that the SD structure was preserved within the volume-filling sPS spherulites. Owing to a small difference in the refractive index between sPS dense and sPS less dense domains, light scattering was found to be not as effective as optical microscopy in detecting the phase-separated morphology. The interplay between the phase separation and cold crystallization gives rise to the presence of a striking minimum of Hv invariant at 150 °C.

Acknowledgements

Financial support by the National Science Council, ROC, under Grant NSC92-2216-E-006-016 is highly appreciated.

References

[1] Guerra G, Vitagliano VM, De Rosa C, Petraccone V, Corradini P. Macromolecules 1990;23:1539.
[2] De Rosa C, De Ballesteros OR, Di Gennaro M, Auriemma F. Polymer 2003;44:1861.
[3] Wang C, Chen CC, Cheng YW, Liao WP, Wang ML. Polymer 2002;43:5271.
[4] Wang C, Chen CC, Hung CH, Lin KS. Polymer 2004;45:6681.
[5] Lawarence SST, Shinozaki DM. Polym Eng Sci 1997;37:1825.
[6] Wu FS, Woo EM. Polym Eng Sci 1999;39:825.
[7] Duff S, Tsuyama S, Iwamoto T, Fujibayashi F, Birkinshaw C. Polymer 2001;42:991.
[8] Chiu FC, Peng CG. Polymer 2002;43:4879.
[9] Cimmino S, Di Pace E, Martuscelli E, Silvestre C. Polym Commun 1991;32:251.
[10] Woo EM, Wu FS. J Polym Sci, Polym Phys Ed 1998;36:2725.
[11] Wang C, Liao WP, Wang ML, Lin CC. Polymer 2004;45:973.
[12] Imai M, Mori K, Mizukami T, Kaji K, Kanaya T. Polymer 1992;33:4451.
[13] Ezquerra TA, López-Cabarcos E, Hsiao BS, Baltà-Calleja FJ. Phys Rev E 1996;54:989.
[14] Terrill NJ, Fairclough PA, Towns-Andrews E, Komanschek BU, Young RJ, Ryan AJ. Polymer 1998;39:2381.
[15] Olmsted PD, Poon WK, McLeish TCB, Terrill NJ, Ryan AJ. Phys Rev Lett 1998;81:373.
[16] Heeley EL, Maidens AV, Olmsted PD, Bras W, Dolbnya IP, Fairclough JPA, et al. Macromolecules 2003;36:3656.
[17] Matsuba G, Kaji K, Kanaya T, Nishida K. Phys Rev E 2002;65:061801.
[18] Wang ZG, Hsiao BS, Srinivas S, Brown GM, Tsou AH, Cheng SZD, et al. Polymer 2001;42:7561.
[19] Matsuba G, Kaji K, Nishida K, Kanaya T, Imai M. Macromolecules 1999;32:8932.
[20] Reynolds NM, Stidham HD, Hsu SL. Macromolecules 1991;24:3662.
[21] Musto P, Tavone S, Guerra G, De Rosa C. J Polym Sci, Polym Phys Ed 1997;35:1055.
[22] Stein RS, Rhodes MB. J Appl Phys 1960;31:1873.
[23] Koberstein J, Russell TP, Stein RS. J Polym Sci, Polym Phys Ed 1979;7:1719.
[24] Avrami M. J Chem Phys 1930;7:1109.
[25] Hoffman JD, Miller RL. Polymer 1997;38:3151.
[26] Suzuki T, Kovacs AJ. Polym J 1970;1:82.
[27] Miyamoto J, Tanzawa Y, Miyaji H, Koho H. Polymer 1992;33:2496.
[28] Okamoto M, Kubo H, Kotaka T. Macromolecules 1999;32:6206.
[29] Santangelo PG, Roland CM. Macromolecules 1998;31:4581.
[30] Natesan B, Xu H, Ince BS, Cebe P. J Polym Sci, Polym Phys Ed 2004;42:777.
[31] Mandelkern L. Physical properties of polymers. 3rd ed. Cambridge: Cambridge University Press; 2004 [Chapter 4].
[32] Nishida K, Kaji K, Kanaya T, Matsuba G, Konishi T. J Polym Sci, Polym Phys Ed 2004;42:1817.
[33] Akpalu Y, Kielhorn L, Hsiao BS, Stein RS, Russell TP, van Egmond J, et al. Macromolecules 1999;32:765.
[34] Petraccone V, Auriemma F, Dal Poggetto F, De Rosa C, Guerra G, Corradini P. Makromol Chem 1993;194:1335.
[35] Sun YS, Woo EM. Polymer 2001;42:2241.
[36] Handa YP, Zhang Z, Wong B. Macromolecules 1997;30:8499.
[37] Auriemma F, Petraccone V, Poggeto FD, De Rosa C, Guerra G, Manfredi C, et al. Macromolecules 1993;26:3772.
[38] Wang C, Liao WP, Cheng YW. J Polym Sci, Polym Phys Ed 2003;41:2457.
[39] Pogodina NV, Siddiquee SK, van Egmond JW, Winter HH. Macromolecules 1999;32:1167.
[40] Debey D, Bueche AM. J Appl Phys 1949;20:518.
[41] Inaba N, Sato K, Suzuki S, Hashimoto T. Macromolecules 1986;19:1690.